Published as: *Mol Cell*. 2008 September 5; 31(5): 631–640.

Lymphocyte-Specific Compensation For XLF/Cernunnos End-Joining Functions In V(D)J Recombination

Gang Li[*], **Frederick W. Alt**[#], **Hwei-Ling Cheng**, **James W. Brush**, **Peter Goff**, **Mike M. Murphy**, **Sonia Franco**, **Yu Zhang**, and **Shan Zha**[*]
Howard Hughes Medical Institute, The Children's Hospital, The CBR institute of Biomedical Research, Harvard Medical School, Boston, MA 02115

SUMMARY

Mutations in XLF/Cernunnos (hereafter called "XLF") cause lymphocytopenia in humans, and various studies suggest an XLF role in classical non-homologous end joining (C-NHEJ). We now find that XLF-deficient mouse embryonic fibroblasts are ionizing radiation (IR) sensitive and severely impaired for ability to support V(D)J recombination. Yet, mature lymphocyte numbers in XLF-deficient mice are only modestly decreased. Moreover, XLF-deficient pro-B lines, while IR-sensitive, carry out V(D)J recombination at nearly wild-type levels. Correspondingly, XLF/p53-double-deficient mice are not markedly prone to the pro-B lymphomas that occur in previously characterized C-NHEJ/p53-deficient mice; however, like other C-NHEJ/p53-deficient mice they still develop medulloblastomas. Despite nearly normal V(D)J recombination in developing B cells, XLF-deficient mature B cells are moderately defective for IgH class switch recombination. Together, our results implicate XLF as a C-NHEJ factor, but also indicate that developing mouse lymphocytes harbor cell type specific factors/pathways that compensate for absence of XLF function during V(D)J recombination.

INTRODUCTION

The classical non-homologous end-joining (C-NHEJ) pathway is critical for repair of general DNA double strand breaks (DSBs) in mammalian cells and for repair of programmed DSBs during lymphocyte development. There are six well-characterized C-NHEJ factors (Dudley et al., 2005), and another, XLF, that was discovered more recently (Ahnesorg et al., 2006; Buck et al., 2006). The Ku80/Ku70 heterodimer (Ku) binds DSBs where, among other functions, it recruits downstream C-NHEJ factors. DNA bound Ku forms a complex with and activates the DNA-dependent protein kinase catalytic subunit (DNA-PKcs), which activates endonuclease activity of Artemis (Goodarzi et al., 2006; Ma et al., 2002; Moshous et al., 2001). The Artemis endonuclease processes a subset of DNA ends to prepare them for end joining (Rooney et al., 2002). Finally, DNA Ligase IV (Lig4), in association with XRCC4, carries out end-ligation. Ku70, Ku80, XRCC4, and Lig4 are considered "core" C-NHEJ factors because they are conserved in evolution and required for all known C-NHEJ reactions; whereas DNA-PKcs and Artemis evolved more recently and are particularly important for joining ends that require processing (Dudley et al., 2005).

#To whom correspondence should be addressed (alt@enders.tch.harvard.edu).
*These authors contributed equally.

Developing B and T lymphocytes assemble Immunoglobulin (Ig) and T cell receptor (TCR) variable region exons from variable (V), diversity (D) and joining (J) gene segments via V(D)J recombination. V(D)J recombination is initiated by the Recombination Activating Gene (RAG) 1 and 2 endonuclease, which introduces DSBs between participating V, D, or J coding sequences and flanking recombination signal (RS) sequences. RAG-mediated cleavage produces two blunt 5′ phosphorylated RS ends and two covalently-sealed (hairpin) coding ends. Subsequently, C-NHEJ fuses the RS ends and the coding ends to form, respectively, RS and coding joins (Dudley et al., 2005). Core C-NHEJ factors are required for both coding and RS joins; while DNA-PKcs and Artemis largely are not required for blunt ligation of RS ends, but are required for coding join formation, due to their role in opening and processing hairpin intermediates (Dudley et al., 2005).

Mature B cells undergo Ig heavy chain (IgH) class switch recombination (CSR), a process that replaces the Cμ IgH constant region (C_H) exons with downstream C_H exons. Long switch (S) regions that precede C_H exons are targets for Activation Induced Cytidine Deaminase (AID), an enzyme that introduces DNA lesions that lead to DSBs (Stavnezer et al., 2008). DSBs in the donor S region upstream of Cμ (Sμ) are joined to DSBs in a downstream acceptor S region to complete CSR. A substantial fraction of normal CSR joins are generated by C-NHEJ, which joins ends that lack homology to form "direct" joins and also joins ends with several base-pair homologies to form microhomology (MH) joins (Yan et al., 2007). Thus, C-NHEJ-deficient B lymphocytes activated for CSR accumulate *IgH* locus chromosomal breaks and translocations due to inability to join broken S regions (Franco et al., 2008; Yan et al., 2007). However, while XRCC4 and Lig4 are absolutely required for V(D)J recombination, substantial CSR (up to 50% of normal levels) occurs in their absence due to an alternative end-joining (A-EJ) pathway that strongly prefers to join ends with MH (Yan et al., 2007). DNA-PKcs deficiency results in variably decreased CSR, and Artemis deficiency has little effect on CSR, likely in part because many broken S region ends do not require processing (Dudley et al., 2005). However, both factors are required for some CSR joins, as their absence leads to *IgH* locus breaks in activated B cells (Franco et al., 2008).

Deficiency in mice for any of the six well-characterized C-NHEJ factors results in severe combined immunodeficiency (SCID) owing to inability to complete V(D)J recombination (Dudley et al., 2005). In addition, deficiency for these C-NHEJ factors results in increased cellular ionizing-radiation (IR) sensitivity and genomic instability. Deficiency for XRCC4, Lig4 and Ku also leads to neuronal apoptosis, which, in the case of XRCC4 and Lig4-deficiency, is so severe that it causes late embryonic lethality (Lee and McKinnon, 2006). V(D)J recombination is not completely blocked in Ku70 or Artemis deficient mice leading to a "leaky" SCID phenotype with very small populations of mature T cells (Dudley et al., 2005). Mice that are doubly deficient for any of the six characterized C-NHEJ factors plus the p53 checkpoint protein succumb to pro-B cell lymphomas, which routinely harbor RAG dependent translocations between *IgH* and chromosomal regions near the *c-myc* or *N-myc* oncogenes (Dudley et al., 2005). While they routinely die from pro-B lymphoma, C-NHEJ/p53 deficient mice also develop medulloblastomas *in situ* (Lee and McKinnon, 2002), and specific deletion of XRCC4 in p53-deficient developing neurons leads to aggressive medulloblastomas with recurrent chromosomal translocations, reflecting the neuronal DSB repair defect (Yan et al., 2006).

Artemis mutations in humans lead to SCID (Moshous et al., 2001). In contrast, XLF mutations in human lead to microcephaly and a combined immunodeficiency that is less severe than that associated with Artemis mutations (Ahnesorg et al., 2006; Buck et al., 2006; Dai et al., 2003). XLF-deficient human fibroblasts (Buck et al., 2006; Dai et al., 2003) and mouse ES cells (Zha et al., 2007) are IR sensitive and have DSB repair defects including severely impaired V(D)J coding and RS joining on episomal substrates. XLF shares structural features with

XRCC4, including an N-terminal head domain and a C-terminal coiled-coil domain required for homo-dimer formation (Ahnesorg et al., 2006; Andres et al., 2007; Li et al., 2007). XLF interacts with XRCC4 (Ahnesorg et al., 2006) and boosts end ligation efficiency of the XRCC4/Lig4 complex *in vitro* (Gu et al., 2007; Lu et al., 2007). XLF also stimulates end joining of mismatched non-cohesive ends and blunt ends, but has little impact on ligation of cohesive ends (Tsai et al., 2007). XLF has an apparent yeast homolog, termed Nej1 (Callebaut et al., 2006; Hentges et al., 2006), which interacts with Lif1p, the yeast homolog of XRCC4 (Teo and Jackson, 2000), suggesting XLF is a "core" C-NHEJ factor. While a role of XLF in C-NHEJ might explain the lymphocytopenia of human XLF-mutant patients, the reason for their relatively mildly impaired lymphocyte development is not clear. Also, one XLF mutant patient was diagnosed with hyper IgM syndrome, suggesting an XLF role in CSR (Buck et al., 2006). To further elucidate XLF function, we now have generated and characterized XLF-mutant mice.

RESULTS

Generation of XLF-Deficient Mice

To characterize XLF function in mouse cells, we employed gene-targeted mutation to delete exons 4 and 5 from both copies of the *Xlf* gene in ES cells (Zha et al., 2007). The resulting $XLF^{\Delta/\Delta}$ ES cells were severely impaired for ability to form V(D)J coding and RS joins in transient assays and were IR-sensitive (Zha et al., 2007). Expression of a wild-type (WT) XLF cDNA rescued IR-sensitivity and defective V(D)J recombination in $XLF^{\Delta/\Delta}$ ES cells, confirming the specificity of the XLF targeting (Zha et al., 2007). Our targeting strategy allowed in-frame splicing from *XLF* exon 3 to 6 to generate a truncated XLF transcript that was readily detectable (Zha et al., 2007). Despite truncated XLF transcripts, a cross-reactive XLF protein was not detected in $XLF^{\Delta/\Delta}$ ES cell extracts (Zha et al., 2007). However, when large amounts of extract from $XLF^{\Delta/\Delta}$ cells were assayed, we sometimes detected very low levels of an XLF cross-reactive band of the approximate size predicted for truncated XLF protein (see below). To estimate maximal levels the putative XLF protein fragment in $XLF^{\Delta/\Delta}$ ES cells relative to those of authentic XLF in WT ES cells, we performed serial dilutions of WT extracts. Based on such experiments, maximal levels of truncated XLF in $XLF^{\Delta/\Delta}$ ES cells, if present at all, generally appeared less than 1% of WT XLF levels (Fig. 1A; Sup. Fig. 1).

The crystal structure of XLF (Andres et al., 2007; Li et al., 2007) reveals that the potential truncated XLF protein generated by our targeting (lacking aa 131 to 196) would lack the α4 (aa 128 to 171) and α5 (aa 171 to 185) regions, which form the coiled-coil domain required for XLF homo-dimerization, and, indirectly, for XRCC4 interaction (Andres et al., 2007; Li et al., 2007). Thus, this truncated XLF protein (referred to as $XLF^{\Delta\alpha4/5}$) potentially would be non-functional. To test for $XLF^{\Delta\alpha4/5}$ activity, we asked whether highly over-expressing an $XLF^{\Delta\alpha4/5}$ cDNA in $XLF^{\Delta/\Delta}$ ES cells complemented IR-sensitivity or defective V(D)J recombination. For this purpose, we introduced a PGK promoter-driven $XLF^{\Delta\alpha4/5}$ cDNA expression vector into $XLF^{\Delta/\Delta}$ ES cells and isolated clones with different copy numbers. Enforced $XLF^{\Delta\alpha4/5}$ cDNA expression generated an XLF cross-reactive protein of the size predicted for $XLF^{\Delta\alpha4/5}$, with the highest copy number lines expressing $XLF^{\Delta\alpha4/5}$ at levels up to 30–40% those of XLF in WT ES cells (Fig. 1A) and which were at least 50 to 100 fold higher than those of $XLF^{\Delta\alpha4/5}$ potentially expressed in $XLF^{\Delta/\Delta}$ cells (Fig. 1A; Sup. Fig. S1; See below). However, even such high level over-expression of $XLF^{\Delta\alpha4/5}$ did not detectably rescue IR sensitivity (Fig. 1B) or V(D)J recombination defects of $XLF^{\Delta/\Delta}$ ES cells (Fig. 1C, Sup. Table S1). Therefore, we conclude that $XLF^{\Delta\alpha4/5}$ only accumulates to very low levels in $XLF^{\Delta/\Delta}$ ES; and, in any case, it is not functional when highly over-expressed. Thus, by available criteria, our targeting appears to generate a functionally null allele.

Three independent $XLF^{+/\Delta}$ ES cell clones were injected for germline transmission and resulting $XLF^{+/\Delta}$ mice bred to generate $XLF^{\Delta/\Delta}$ mice in a 129/Sv background. $XLF^{\Delta/\Delta}$ mice were fertile, born at Mendelian ratios and were normal in size (data not shown). Western blotting analyses confirmed undetectable or very low level expression of an anti-XLF cross-reactive band of the size predicted for $XLF^{\Delta\alpha4}$ in various tissues of $XLF^{\Delta/\Delta}$ mice (see below). While the human XLF mutation is associated with microcephaly and Ku-, XRCC4-, and Lig4 deficiency with increased apoptosis of developing neurons in mice, we did not observe excessive neuronal cell death or a significant reduction of brain weight in embryonic (E17.5; n=3) and adult (P30; n=3) $XLF^{\Delta/\Delta}$ mice (Sup. Fig. S2). We also did not observe overt malignancies including thymic lymphomas in a cohort (n=18) of $XLF^{\Delta/\Delta}$ deficient mice followed for 18 months (data not shown). $XLF^{+/\Delta}$ cells and mice were indistinguishable from WT, excluding dominant negative effects of the XLF^{Δ} allele (data not shown).

Increased IR Sensitivity and Impaired V(D)J Recombination in $XLF^{\Delta/\Delta}$ MEFs

We generated mouse embryonic fibroblasts (MEFs) from day 13.5 $XLF^{\Delta/\Delta}$ and littermate control (WT) embryos. Proliferation of $XLF^{\Delta/\Delta}$ MEFs was indistinguishable from that of WT MEFs derived from both inbred (pure 129/Sv, set a) and mixed (129/BL6 mixed, set b) backgrounds (Fig. 2A). Consistent with findings on $XLF^{\Delta/\Delta}$ ES cells, $XLF^{\Delta/\Delta}$ MEFs exhibited substantially increased IR sensitivity compared to WT controls (Fig. 2B). Furthermore, telomere- FISH (T-FISH) revealed that 13±3% of metaphases from $XLF^{\Delta/\Delta}$ MEFs had at least one chromosomal break, in comparison to 1±2% in metaphases from WT MEFs (Fig. 2C left panel). Almost all chromosomal breaks in $XLF^{\Delta/\Delta}$ MEFs were chromosome breaks, as opposed to chromatid breaks (Fig. 2C; right panel), similar to the distribution of chromosomal abnormalities associated with deficiency for various C-NHEJ factors (Franco et al., 2008;Li et al., 2007;Mills et al., 2004;Yan et al., 2007).

SV40 Large T-antigen immortalized $XLF^{\Delta/\Delta}$ MEFs had substantially reduced ability to generate V(D)J coding or RS joins (5–20% of wild type levels), as measured by three independent transient V(D)J assays on two sets of $XLF^{\Delta/\Delta}$ and WT littermate MEFs (Fig. 2D and Sup. Table S2). Notably, while residual coding joins recovered from transient assays of other C-NHEJ deficient cells are mostly aberrant (e.g. large deletions), residual coding joins recovered from $XLF^{\Delta/\Delta}$ MEFs, like those from $XLF^{\Delta/\Delta}$ ES cells, resembled those of WT MEFs in terms of length and junctional modifications (Sup. Fig. S3). Similarly, 80% of the residual RS joins recovered from $XLF^{\Delta/\Delta}$ MEFs were precise (Fig. 2D). We conclude that $XLF^{\Delta/\Delta}$ MEFs generally resemble $XLF^{\Delta/\Delta}$ ES cells with respect to IR sensitivity, defective V(D)J recombination in transient assays, and increased genomic instability.

Lymphocyte Development in $XLF^{\Delta/\Delta}$ Mice

Western blot analyses of extracts from total thymus, spleen, and bone marrow of $XLF^{\Delta/\Delta}$ mice showed that expression of putative $XLF^{\Delta\alpha4/5}$ protein occurred at levels ranging from undetectable (in some experiments titrating to less than 0.2% of authentic XLF levels in WT extracts) to very weakly detectable (less than 1% of levels of WT XLF) (Fig. 3A; Sup. Fig. S1). Total cell numbers in the thymus and spleens of four-week old $XLF^{\Delta/\Delta}$ mice were, on average, about 40–50% those of WT (Fig. 3C). However, flow cytometry revealed that distribution of pro-B ($CD43^+B220^+IgM^-$), pre-B ($CD43^-B220^+IgM^-$), newly generated B (IgM^+B220^{low}) and re-circulating B (IgM^+B220^{hi}) cells in $XLF^{\Delta/\Delta}$ bone marrow were similar to those of WT and $XLF^{+/\Delta}$ littermates (Fig. 3B and 3C). In addition, $XLF^{\Delta/\Delta}$ mice contained splenic IgM^+ B cells at numbers approximately 30–50% those of WT (Fig. 3B and 3C). Similarly, despite the mild reduction in total thymocyte numbers, the distribution of $CD4^-CD8^-$ (double negative or DN), $CD4^+/CD8^+$ (double positive or DP) and $CD4^+/CD8^-$ or $CD8^+/CD4^-$ (single positive or SP) $XLF^{\Delta/\Delta}$ thymocytes was comparable to those of WT littermates (Fig. 3B and 3C). Reduced levels of surface CD3 and TCRβ expression in

$ATM^{-/-}$ thymocytes (Borghesani et al., 2000) might reflect a modestly impaired V(D)J recombination (Huang et al., 2006). In this regard, $XLF^{\Delta/\Delta}$ and WT thymocytes express similar surface CD3 and TCRβ levels (Sup. Fig. S4). $XLF^{\Delta/\Delta}$ mice also contained normal populations of splenic SP ($CD4^+CD8^-$ and $CD4^-CD8^+$) T cells (Fig. 3B and 3C). Finally, comparative analyses of spleens, bone marrow, and thymus of four-month and eight-month old $XLF^{\Delta/\Delta}$ mice and their WT littermates did not reveal obvious differences in distributions of developing and mature B and T cell populations (Sup. Fig. S5).

V(D)J recombination is initiated in developing B and T lineage cells, respectively, at the pro-B ($CD43^+B220^+IgM^-$) and DN thymocyte ($CD4^-CD8^-$) stages. Correspondingly, B and T cell development is blocked at the pro-B and DN T cell stages in RAG2 deficient mice (Fig. 3B and 3C) (Shinkai et al., 1992), and in all previously characterized C-NHEJ-deficient mice (Dudley et al., 2005), owing to inability to initiate or complete V(D)J recombination. Therefore, the relatively normal distribution of $XLF^{\Delta/\Delta}$ B and T cell populations beyond these stages suggests that V(D)J recombination occurs at relatively normal levels in developing $XLF^{\Delta/\Delta}$ lymphocytes, despite the substantial impairment of this process in $XLF^{\Delta/\Delta}$ ES cells and MEFs. To further address this possibility, we used a PCR approach to isolate thymocyte TCRβ junctions and splenocyte IgH locus V(D)J junctions from $XLF^{\Delta/\Delta}$ and littermate control mice. Notably, all junctions recovered from $XLF^{\Delta/\Delta}$ lymphocytes, whether in frame or out of frame (*e.g.* not influenced by cellular selection), were similar to those recovered from corresponding populations of WT lymphocytes (Sup. Fig. S6 and S7). In contrast, normal V(D)J junctions were not readily isolated from previously analyzed C-NHEJ-deficient mice (Dudley et al., 2005). Overall, our findings suggest that V(D)J recombination occurs relatively normally at endogenous loci of developing $XLF^{\Delta/\Delta}$ lymphocytes.

V(D)J Recombination of Transient and Chromosomal V(D)J Recombination Substrates in $XLF^{\Delta/\Delta}$ Pro-B Cell Lines

$XLF^{\Delta/\Delta}$ developing B and T cells perform relatively normal V(D)J recombination of endogenous antigen receptor loci, despite severe V(D)J recombination defects of $XLF^{\Delta/\Delta}$ MEFs and ES cells as assayed by episomal substrates. Potential explanations for these apparently contradictory findings include XLF being required only for extrachromosomal V(D)J recombination or developing lymphocytes having properties that allow V(D)J recombination in the absence of XLF. To distinguish between these possibilities, we generated Eμ-Bcl2 transgenic Abelson Murine Leukemia Virus (A-MuLV) transformed pro-B cell lines from WT, $XRCC4^{-/-}$ and $XLF^{\Delta/\Delta}$ mice. Treatment of such lines with STI571 arrests them in the G1, induces RAG1/2 expression, and induces V(D)J recombination of chromosomally integrated substrates (Bredemeyer et al., 2006).

Western blotting confirmed lack of normal XLF protein in multiple tested $XLF^{\Delta/\Delta}$ A-MuLV transformants and titrations indicated that, when detected, the putative $XLF^{\Delta\alpha4/5}$ band was at less than 0.2% WT XLF levels (Fig. 4A; Sup. Fig. 1). To confirm absence of physiologically active XLF, we tested for IR-sensitivity and found that $XLF^{\Delta/\Delta}$ lines (n=6) had increased IR sensitivity compared to WT and that this sensitivity was rescued by ectopic over-expression of WT XLF (Fig. 4B and data not shown). While it is difficult to directly compare IR sensitivity of different cell types, the IR sensitivity of $XLF^{\Delta/\Delta}$ A-MuLV transformants, like that of $XLF^{\Delta/\Delta}$ ES cells (Fig. 1), is greater than that of the corresponding WT cells but less than that of corresponding XRCC4 deficient cells. To directly assay for DSB repair, we measured DNA fragmentation at different time points after IR in WT, $XLF^{\Delta/\Delta}$, and $XRCC4^{-/-}$ A-MuLV transformants by pulse-field gel electrophoresis. Notably, $XLF^{\Delta/\Delta}$ cells, similar to XRCC4 deficient A-MuLV transformants, showed impairments in both the rate and the extent of DNA DSB repair as compared to WT A-MuLV transformants (Fig. 4C). Ectopic over-expression of

XLF also rescued DSB repair defects of XLF$^{\Delta/\Delta}$ A-MuLV transformants, demonstrating that the defect in XLF$^{\Delta/\Delta}$ cells is XLF-specific (Fig. 4B and C).

We employed transient transfection assays to test ability of XLF$^{\Delta/\Delta}$ A-MuLV transformants to perform V(D)J recombination on extrachromosomal substrates and found that, within the sensitivity of this assay, they generated coding and RS joins at efficiencies indistinguishable from those of WT (Fig. 4D and Sup. Fig. S8 and Table S3). Sequences of coding junctions from XLF$^{\Delta/\Delta}$ transformants also were indistinguishable from those of WT (Table S2). On the other hand, about 15% of XLF$^{\Delta/\Delta}$ RS junctions were imprecise, as opposed to 100% fidelity of RS junctions from WT A-MuLV transformants (Sup. Fig. S8). Therefore, in XLF$^{\Delta/\Delta}$ A-MuLV transformants, we find no measurable defect in V(D)J recombination levels and only a slight defect in the quality of V(D)J RS junctions as measured *via* episomal substrates.

To test whether XLF$^{\Delta/\Delta}$ A-MuLV transformants are defective in chromosomal V(D)J recombination, we generated XLF$^{\Delta/\Delta}$ and WT A-MuLV transformants that harbored a single chromosomally integrated copy of an inversional V(D)J substrate that activates GFP expression following successful V(D)J recombination (Bredemeyer et al., 2006). A substantial proportion of XLF$^{\Delta/\Delta}$ and WT A-MuLV transformants rearranged the integrated V(D)J substrates, as measured by GFP expression at 48 and 96 hours after STI571 treatment (Fig. 5A; Sup. Fig. 9). In contrast, no GFP positive XRCC4$^{-/-}$ A-MuLV transformants were observed at either time point, consistent with their severe NHEJ defects (Fig. 5A; Sup. Fig. 9). Southern blotting confirmed substantial rearrangement of the integrated substrates in WT and XLF$^{\Delta/\Delta}$ A-MuLV transformants and absence of detectable rearrangements in XRCC4$^{-/-}$ A-MuLV transformants (Fig. 5B; Sup. Fig. 9). Correspondingly, while Southern blotting revealed readily detectable levels of broken coding ends (3' coding ends) in STI571-treated XRCC4$^{-/-}$ A-MuLV transformants; such broken coding ends were not detected in WT A-MuLV transformants and were detected only at low levels in a subset of XLF$^{\Delta/\Delta}$ A-MuLV transformants (Fig 5B; Sup. Fig. 9). Together, our findings indicate that XLF$^{\Delta/\Delta}$ A-MuLV transformants support V(D)J recombination on both episomal and chromosomally integrated V(D)J recombination substrates at levels approaching those of WT.

Pro-B cell Lymphoma is Rare in XLF$^{\Delta/\Delta}$p53$^{-/-}$ Mice

We generated a cohort of XLF$^{\Delta/\Delta}$p53$^{-/-}$ mice to test whether XLF suppresses oncogenic translocations in developing lymphocytes and neurons. In striking contrast to all previously characterized C-NHEJ/p53 double deficient mice, the vast majority (20/21) of XLF$^{\Delta/\Delta}$p53$^{-/-}$ mice succumbed to thymic lymphoma (median survival =102.5 day; Sup. Fig. 10), that, in those characterized, lacked clonal translocations; and, thus, appeared to represent thymic lymphomas resulting from p53-deficiency alone (Sup. Fig. 10). Only one of the 21 XLF$^{\Delta/\Delta}$p53$^{-/-}$ mice succumbed to pro-B lymphoma. This XLF$^{\Delta/\Delta}$p53$^{-/-}$ pro-B lymphoma contained a clonal 12/15 translocation and amplified J_H and *c-Myc* loci as routinely observed in pro-B lymphomas from other C-NHEJ/p53-deficient mice (Sup. Fig. 10). On the other hand, histological analyses of brain samples from eight XLF$^{\Delta/\Delta}$p53$^{-/-}$ mice that died of thymic lymphoma revealed that 6 of 8 had medulloblastoma *in situ* (Sup. Fig. 10), as previously observed in various other C-NHEJ/p53 double deficient mice (Lee and McKinnon, 2002). Thus, XLF deficiency in a p53 deficient background rarely leads to pro-B lymphomas, but frequently leads to medulloblastomas. As the pro-B lymphomas in other C-NHEJ/p53 deficient backgrounds are associated with RAG-dependent oncogenic translocations, these findings are consistent with developing XLF$^{\Delta/\Delta}$ pro-B cells lacking a severe V(D)J recombination defect.

CSR Defects in XLF$^{\Delta/\Delta}$ B Cells

To assay for potential CSR defects associated with XLF-deficiency, we purified XLF$^{\Delta/\Delta}$ and WT CD43^{-} splenic B cells and activated them for four days, respectively with anti-CD40 plus

interleukin 4 (IL-4) to induce CSR to IgG1 or with bacterial lipopolysaccharide (LPS) to induce CSR to IgG3. Proliferation of $XLF^{\Delta/\Delta}$ B cells, under either type of stimulation, was similar to that of WT B cells (Fig. 6A; data not shown). After four days of stimulation, switching to these IgG1 or IgG3 was measured by surface expression. Following anti-CD40 plus IL-4 stimulation, approximately 44% of WT B cells and 23% $XLF^{\Delta/\Delta}$ B cells became $IgG1^{+}$ (n=6 independent stimulations) (Fig. 6B). Following LPS stimulation, approximately 9% of WT B cells and 5% $XLF^{\Delta/\Delta}$ B cells became $IgG3^{+}$ (n=4 independent stimulations) (Fig. 6B). Similar results were obtained from hybridoma analyses (Sup. Fig. 11). Total serum IgM levels of $XLF^{\Delta/\Delta}$ mice appeared slightly increased; while serum IgG1 and IgG3 levels in $XLF^{\Delta/\Delta}$ mice were significantly decreased as compared to those of age matched WT mice, consistent with the CSR defects observed *in vitro* (Sup. Fig. 11).

While the surface staining studies demonstrate that $XLF^{\Delta/\Delta}$ B cells are defective for IgH CSR, they do not show that the defect occurs at the level of joining. However, even modest CSR joining defects can be identified by an IgH locus FISH assay that reveals IgH locus-specific chromosomal breaks (Franco et al., 2008). Assays for IgH locus breaks in anti-CD40/IL-stimulated $XLF^{\Delta/\Delta}$ and WT control B cells revealed a substantial CSR joining defect in $XLF^{\Delta/\Delta}$ B cells, as about 9% of the $XLF^{\Delta/\Delta}$ B cell metaphases contained IgH specific chromosomal breaks, as compared to about 2% for WT B metaphases (Fig. 6C; n=4 independent experiments, p-value= 0.002;). Moreover, AID-deficiency eliminated the IgH locus breaks in anti-CD40/IL-4 activated $XLF^{\Delta/\Delta}$ B cells (Fig. 6C and Sup. Fig. 10), demonstrating that they result from failure to complete CSR. LPS stimulated $XLF^{\Delta/\Delta}$ B cells did not accumulate any detectable IgH locus specific breaks, probably because LPS-activated B cells with unrepaired breaks are eliminated by a p53 dependent mechanism (Sup. Fig. 11) (Franco et al., 2008). To further elucidate the IgH CSR defect in $XLF^{\Delta/\Delta}$ cells, we amplified and sequenced Sμ–Sγ1 junctions from IgG1 positive $XLF^{\Delta/\Delta}$ and WT B cells. In contrast to XRCC4 deficient B cells, which lack "direct" CSR junctions (Yan et al., 2007), $XLF^{\Delta/\Delta}$ B cells had a significant frequency of direct CSR joins; although the number appeared potentially less than that of WT B cells (14% *vs* 23%; Sup. Fig. 11). Correspondingly, an increased proportion of the $XLF^{\Delta/\Delta}$ B cell CSR junctions had MHs; and, on average, the MHs in $XLF^{\Delta/\Delta}$ CSR junctions were longer (Sup. Fig. 11).

DISCUSSION

XLF was proposed to be a core member of the C-NHEJ pathway (Ahnesorg et al., 2006; Buck et al., 2006; Dai et al., 2003). Correspondingly, we now show that $XLF^{\Delta/\Delta}$ mice share many phenotypic features found in other C-NHEJ deficiencies. In this regard, $XLF^{\Delta/\Delta}$ MEFs and pro-B cell lines are IR sensitive, have substantial genomic instability, and have major defects in ability to repair IR-induced DSBs. Similarly, $XLF^{\Delta/\Delta}$ mature B cells are markedly defective in ability to repair chromosomal breaks during IgH CSR. In addition, XLF/p53 deficient mice, like XRCC4/p53 or Lig4/p53 deficient mice, develop medulloblastoma *in situ*, likely reflecting unrepaired DSBs in neuronal cells. Yet, we find, surprisingly, that $XLF^{\Delta/\Delta}$ mice have a lymphocyte developmental phenotype that is distinct from that of all other characterized C-NHEJ deficiencies. Specifically, $XLF^{\Delta/\Delta}$ mice have relatively unimpaired lymphocyte development; $XLF^{\Delta/\Delta}$ pro-B cell lines support nearly normal V(D)J recombination despite being IR sensitive and defective in general DSB repair; and XLF/p53 deficient mice are not markedly prone to pro- B lymphomas. Together, these findings support a fundamental role of XLF in C-NHEJ and further suggest that developing lymphocytes contain increased relative activity of a compensatory pathway/factor, as compared to other analyzed cell types, which supports relatively normal V(D)J recombination in the absence of XLF.

Function of XLF and the Putative XLF Compensatory Factor

Spontaneous genomic instability in $XLF^{\Delta/\Delta}$ cells mainly occurs as chromosome breaks (Fig. 2C), suggesting that XLF, like previously characterized C-NHEJ factors, functions mainly in the repair of pre-replicative DSBs. While XLF deficient MEFs show severe defects in both coding and RS joining in the context of transient V(D)J recombination assays, residual levels of both types of V(D)J recombination joind are greater than those of XRCC4 or Lig4 deficient MEFs (Fig. 2D) (Frank et al., 1998;Gao et al., 1998b). Correspondingly, $XLF^{\Delta/\Delta}$ MEFs do not show proliferation or premature senescence defects observed for core C-NHEJ factor deficient MEFs (Frank et al., 1998;Gao et al., 1998b;Nussenzweig et al., 1996). Likewise, $XLF^{\Delta/\Delta}$ ES and pro-B lines, while IR sensitive, are not as sensitive as corresponding XRCC4-deficient lines. While the relatively mild growth and IR-sensitivity of $XLF^{\Delta/\Delta}$ cells are reminiscent of DNA-PKcs- or Artemis-deficient cells (Gao et al., 1998a;Rooney et al., 2002), there are notable differences. First, the V(D)J coding end joining defect is much less severe in $XLF^{\Delta/\Delta}$ cells than in Artemis or DNA-PKcs deficient cells, particularly in developing lymphocytes due to the apparent XLF compensatory mechanism. On the other hand, V(D)J joining of RS ends is much more severely impaired in $XLF^{\Delta/\Delta}$ cells other than lymphocytes (again due to the apparent compensatory mechanism) than in DNA-PKcs and Artemis deficient cells.

What type of activity/process compensates for normal XLF function specifically in V(D)J recombination and specifically in developing lymphocytes? One possibility is a factor that interacts with XRCC4 to directly substitute for XLF function. Alternatively, the compensatory mechanism may be indirect and involve a factor that functions differently, but which negates the requirement for normal XLF function. In this context, given the biochemical demonstration of a preferential requirement for XLF in the joining of certain ends, end-modification factors expressed exclusively or preferentially in developing lymphocytes, such as polymerase family X members (i.e. TdT, Polμ and Polλ) (Weill and Reynaud, 2008) are candidates, given their known role in V(D)J recombination but not in general DSB repair. However, while these proteins can alter V(D)J coding ends and interact with core NHEJ factors, they have no known role in RS joining (Weill and Reynaud, 2008). Other potential candidate factors might include certain DSB response proteins, such as H2AX or ATM, that could somehow function to stabilize or otherwise alter joining of broken V(D)J ends (Bassing et al., 2003; Bredemeyer et al., 2006; Callen et al., 2007; Celeste et al., 2003).

Unlike other core C-NHEJ factor deficient cells, $XLF^{\Delta/\Delta}$ MEFs and ES cells make low levels of apparently normal coding and RS joins. By analogy to DNA-PKcs or Artemis-deficiency, the ability of XLF-deficient non-lymphoid cells to generate low levels of normal V(D)J joins might reflect joining of certain types of ends in the absence of XLF. However, the joining efficiency of RS ends, which are generated as blunt 5′ phosphorylated DSBs, also is impaired in non-lymphoid, but is relatively normal in lymphoid, $XLF^{\Delta/\Delta}$ cells. In addition, characterized V(D)J joins from XLF-deficient cells, thus far, shows no obvious indication of particular end preferences. Therefore, a potentially more attractive possibility would be that non-lymphoid cell types, including MEFs and ES cells, express reduced levels of a putative developing lymphocyte-specific XLF compensatory mechanism that allows normal joining of those ends with which it associates. Such a mechanism might explain similar findings that V(D)J junctions recovered from XLF-mutant human fibroblasts also are largely normal despite the severely reduced V(D)J recombination efficiency (Buck et al., 2006; Dai et al., 2003).

Implications of Mouse Studies for the Phenotype of XLF-Mutations in Humans

In contrast to the SCID of Artemis deficient patients (Moshous et al., 2001), XLF mutated human patients have a variable, often moderate, reduction of peripheral B cell numbers (Buck et al., 2006). In this regard, the human phenotype is reminiscent of that of $XLF^{\Delta/\Delta}$ mice. One possible explanation for substantial numbers of mature lymphocytes in younger XLF-mutant

patients would be that known human mutations do not fully inactivate XLF. However, there are a variety of different XLF mutations and a number might be predicted to inactivate the protein (Buck et al., 2006). Alternatively, based on our current findings with XLF-deficient mice, XLF also might be relatively dispensable for V(D)J recombination in developing human lymphocytes. If so, reduced numbers of human XLF-mutant lymphocytes might in part reflect the role of XLF in general DSB repair, either in progenitor or mature lymphocytes or in hematopoietic stem cells (Rossi et al., 2007). This explanation also may be relevant to the modest reduction in $XLF^{\Delta/\Delta}$ mouse lymphocyte numbers. In this context, IgH and IgL knock-in alleles do not fully rescue lymphocyte numbers in the context of NHEJ deficiencies as compared to RAG deficiency (Casellas et al., 1998) and reduced numbers of developing and peripheral mouse lymphocytes occur in the context of deficiencies for DSB response proteins (e.g. H2AX) that have no major role in V(D)J recombination (Bassing et al., 2003; Celeste et al., 2002).

One XLF mutant patient had a hyper-IgM syndrome, with increased accumulation of IgM and a decrease of other IgH isotypes (Buck et al., 2006); but the underlying mechanism was unclear. Correspondingly, we observe a modest IgM increase with decreased IgG1 and, particularly, IgG3 in serum of $XLF^{\Delta/\Delta}$ mice (Sup. Fig. 11). In this regard, a hyper-IgM syndrome might reflect either CSR or B cell activation defects. Our mouse studies show that XLF, like other C-NHEJ factors, is required for normal CSR levels in mouse B cells. Furthermore, based on our finding of AID-dependent IgH locus chromosomal breaks in $XLF^{\Delta/\Delta}$ cells stimulated for CSR, we conclude that XLF is required for joining a subset of CSR ends. In contrast to B cells deficient for XRCC4, in which CSR is carried out by a pathway extremely biased towards MH-mediated joining (Yan et al., 2007), $XLF^{\Delta/\Delta}$ B cells generate both direct and MH mediated CSR joins, suggesting XLF may not be required for all CSR joins mediated by C-NHEJ.

Ectopic Bcl2 Expression Does not Inhibit V(D)J recombination in Mouse Pro-B Cells

Ectopic Bcl2 expression was shown to impair C-NHEJ and V(D)J recombination on episomal substrates in human cells (Wang et al., 2008). In contrast, we show that ectopic Bcl2 over-expression in WT A-MuLV transformed B cell lines, at levels sufficient to allow the cells to withstand STI571 treatment, had no detectable effect on transient substrate V(D)J recombination including RS joining fidelity (Sup Fig. 8) or on chromosomal V(D)J recombination, as indicated by lack of coding end breaks that are observed in XRCC4 deficient lines (Fig. 5B; Sup Fig. 9). We note that the transient V(D)J substrates used in our assays were identical to those used in studies of Bcl2 over-expressing human cells (Wang et al., 2008). The reason for the discrepancy between the results of our studies and those with Bcl2 over-expressing human cells is unclear; but might reflect cell type differences (lung carcinoma *vs*. lymphocyte), species differences (human vs. mouse), Bcl-2 expression level differences, or other factors. We note, however, that our findings are consistent with prior findings that normal pro-B cells, in which IgH V(D)J recombination occurs, express high Bcl2 levels (Young et al., 1997).

MATERIAL AND METHODS

Generation of XLF-Deficient Mice

$XLF^{+/\Delta}$ ES cells were generated as described (Zha et al., 2007). Three independent $XLF^{+/\Delta}$ ES cell clones were injected into C57/BL6 blastocysts to generate chimeric mice. Founder chimeras were bred to 129/Sv females, and the resulting F1 heterozygotes intercrossed to generate homozygous mutant mice in 129/Sv background. Loss of XLF was confirmed by genomic PCR with three primers: F8244 5'-CAT GTT GGC TCT GCG AAT AGA-3' and R11166 5' GAG TCT GGA TAT GAG CGC TCA G-3' for KO allele; F10642 5' CTG TCT TGT GGG CAT AGT AGG C-3' and R11166 for the WT allele.

Western Blotting

Western blotting was performed using an antibody against the C-terminus of XLF with the reported epitope lying between residue 250 and the C-terminus of human XLF (cat. no. A300–730A-1, Bethyl Laboratories, Montgomery, TX) as described (Zha et al., 2007).

IR Sensitivity Assays

We assayed for IR sensitivity as described (Mostoslavsky et al., 2006). Briefly, we plated about 10^4 P1 MEFs in triplicate on day 0, irradiated with indicated doses using a ^{137}Cs source at day 1 and cultured for 7 days. The percentage of cells in irradiated wells *vs*. untreated wells was plotted as a function of dose. A similar approach was used for A-MuLV transformed pro-B cells. IR sensitivity in ES cells was measured as described (Zha et al., 2007). For growth curves, MEFs were plated in triplicate (2×10^4 cells/12 well-plate well) and counted every other day for 8 days.

Extrachromosomal V(D)J Recombination Assays

Substrates that test coding (pJH290) or RS join formation (pJH200) were transiently transfected into test cells together with full length RAG1 and RAG2 expression vectors as described (Zha et al., 2007). For ES cells, 3×10^6 cells were plated the day before transfection. For MEFs, 1×10^6 cells were used for transfection. For A-MuLV pro-B cells, 30×10^6 cells were used for DEAE-dextran transfection. The fidelity of RS joins and the coding join junctions were analyzed as described (Zha et al., 2007).

Chromosomal V(D)J Recombination Assays in A-MuLV Transformants

V(D)J recombination with an integrated substrate was carried out as described (Bredemeyer et al., 2006). Briefly, A-MuLV transformed pro-B-cell lines were isolated from XLF$^{\Delta/\Delta}$ mice or WT mice that harbored an Eμ-Bcl2 transgene. For XRCC4-deficient A-MuLV transformants, the Eμ-Bcl2 transgene was stably introduced after establishment of the line. The A-MuLV transformed pro-B lines were infected with the pMX-RSS-GFP/IRES-hCD4 (pMX-INV) retroviral vector which was then employed to assay for V(D)J recombination. We identified clones with single copy substrates by Southern blotting. Analyses were done on lines harboring a single copy substrate integration as described previously (Bredemeyer et al., 2006).

Genomic Instability and DNA Double Strand Break Repair Assays

Genomic instability assays on MEFs were performed by T-FISH as described (Mostoslavsky et al., 2006). Briefly 5×10^6 cells were treated with colcemid (100ng/ml) for 3 hours, harvested, and fixed. Metaphase chromosomal aberrations were visualized by staining with a telomere PNA probe and DAPI and analyzed using a Nikon Eclipse microscope.

To measure DNA fragmentation after IR, we harvested 1×10^6 A-MuLV transformants immediately before and at different times after exposure to 80Gy of radiation. Cells were embedded in argrose plugs and analyzed by pulse field gel electrophoresis as described (Mostoslavsky et al., 2006). The fraction of DNA released into the gel was calculated based on densitometry measurements as described (Celeste et al., 2002). The fraction of DNA released into the gel before and after irradiation was set as 0% and 100%, respectively.

Lymphocyte Development and IgH Class Switch Recombination

Lymphocyte populations were analyzed by flow cytometry as described (Rooney et al., 2002). Conditions for isolation and activation of splenic B cells and flow cytometric assays for IgH class switching were done as described (Franco et al., 2006) Two color FISH assays for IgH locus breaks were performed as described (Franco et al., 2006).

Supplementary Material

Refer to Web version on PubMed Central for supplementary material.

ACKNOWLEDGEMENTS

We thank L. Notarangelo and J.P. DeVillartay for critical review of this manuscript. This work was supported by National Institute of Health Grants AI35714 and CA92625 (to F.W.A.). F.W.A. is an investigator and G.L a postdoctoral associate of the Howard Hughes Medical Institute. S.Z. was a fellow and now a senior fellow of the Leukemia and Lymphoma Society. S.F was supported by a long term fellowship from EMBO and Y.Z is a fellow of Cancer Research Institute.

Reference List

Ahnesorg P, Smith P, Jackson SP. XLF interacts with the XRCC4-DNA ligase IV complex to promote DNA nonhomologous end-joining. Cell 2006;124:301–313. [PubMed: 16439205]

Andres SN, Modesti M, Tsai CJ, Chu G, Junop MS. Crystal Structure of Human XLF: A Twist in Nonhomologous DNA End-Joining. Mol. Cell 2007;28:1093–1101. [PubMed: 18158905]

Bassing CH, Suh H, Ferguson DO, Chua KF, Manis J, Eckersdorff M, Gleason M, Bronson R, Lee C, Alt FW. Histone H2AX: a dosage-dependent suppressor of oncogenic translocations and tumors. Cell 2003;114:359–370. [PubMed: 12914700]

Borghesani PR, Alt FW, Bottaro A, Davidson L, Aksoy S, Rathbun GA, Roberts TM, Swat W, Segal RA, Gu Y. Abnormal development of Purkinje cells and lymphocytes in Atm mutant mice. Proc. Natl. Acad. Sci. U. S. A 2000;97:3336–3341. [PubMed: 10716718]

Bredemeyer AL, Sharma GG, Huang CY, Helmink BA, Walker LM, Khor KC, Nuskey B, Sullivan KE, Pandita TK, Bassing CH, Sleckman BP. ATM stabilizes DNA double-strand-break complexes during V(D)J recombination. Nature 2006;442:466–470. [PubMed: 16799570]

Buck D, Malivert L, de Chasseval R, Barraud A, Fondaneche MC, Sanal O, Plebani A, Stephan JL, Hufnagel M, le Deist F, Fischer A, Durandy A, de Villartay JP, Revy P. Cernunnos, a novel nonhomologous end-joining factor, is mutated in human immunodeficiency with microcephaly. Cell 2006;124:287–299. [PubMed: 16439204]

Callebaut I, Malivert L, Fischer A, Mornon JP, Revy P, de Villartay JP. Cernunnos interacts with the XRCC4 x DNA-ligase IV complex and is homologous to the yeast nonhomologous end-joining factor Nej1. J. Biol. Chem 2006;281:13857–13860. [PubMed: 16571728]

Callen E, Jankovic M, Difilippantonio S, Daniel JA, Chen HT, Celeste A, Pellegrini M, McBride K, Wangsa D, Bredemeyer AL, Sleckman BP, Ried T, Nussenzweig M, Nussenzweig A. ATM prevents the persistence and propagation of chromosome breaks in lymphocytes. Cell 2007;130:63–75. [PubMed: 17599403]

Casellas R, Nussenzweig A, Wuerffel R, Pelanda R, Reichlin A, Suh H, Qin XF, Besmer E, Kenter A, Rajewsky K, Nussenzweig MC. Ku80 is required for immunoglobulin isotype switching. EMBO J 1998;17:2404–2411. [PubMed: 9545251]

Celeste A, Difilippantonio S, Difilippantonio MJ, Fernandez-Capetillo O, Pilch DR, Sedelnikova OA, Eckhaus M, Ried T, Bonner WM, Nussenzweig A. H2AX haploinsufficiency modifies genomic stability and tumor susceptibility. Cell 2003;114:371–383. [PubMed: 12914701]

Celeste A, Petersen S, Romanienko PJ, Fernandez-Capetillo O, Chen HT, Sedelnikova OA, Reina-San-Martin B, Coppola V, Meffre E, Difilippantonio MJ, Redon C, Pilch DR, Olaru A, Eckhaus M, Camerini-Otero RD, Tessarollo L, Livak F, Manova K, Bonner WM, Nussenzweig MC, Nussenzweig A. Genomic instability in mice lacking histone H2AX. Science 2002;296:922–927. [PubMed: 11934988]

Dai Y, Kysela B, Hanakahi LA, Manolis K, Riballo E, Stumm M, Harville TO, West SC, Oettinger MA, Jeggo PA. Nonhomologous end joining and V(D)J recombination require an additional factor. Proc. Natl. Acad. Sci. U. S. A 2003;100:2462–2467. [PubMed: 12604777]

Dudley DD, Chaudhuri J, Bassing CH, Alt FW. Mechanism and control of V(D)J recombination versus class switch recombination: similarities and differences. Adv. Immunol 2005;86:43–112. [PubMed: 15705419]

Franco S, Gostissa M, Zha S, Lombard DB, Murphy MM, Zarrin AA, Yan C, Tepsuporn S, Morales JC, Adams MM, Lou Z, Bassing CH, Manis JP, Chen J, Carpenter PB, Alt FW. H2AX prevents DNA breaks from progressing to chromosome breaks and translocations. Mol. Cell 2006;21:201–214. [PubMed: 16427010]

Franco S, Murphy MM, Li G, Borjeson T, Boboila C, Alt FW. DNA-PKcs and Artemis function in the end-joining phase of immunoglobulin heavy chain class switch recombination. J. Exp. Med 2008;205:557–564. [PubMed: 18316419]

Frank KM, Sekiguchi JM, Seidl KJ, Swat W, Rathbun GA, Cheng HL, Davidson L, Kangaloo L, Alt FW. Late embryonic lethality and impaired V(D)J recombination in mice lacking DNA ligase IV. Nature 1998;396:173–177. [PubMed: 9823897]

Gao Y, Chaudhuri J, Zhu C, Davidson L, Weaver DT, Alt FW. A targeted DNA-PKcs-null mutation reveals DNA-PK-independent functions for KU in V(D)J recombination. Immunity 1998a;9:367–376. [PubMed: 9768756]

Gao Y, Sun Y, Frank KM, Dikkes P, Fujiwara Y, Seidl KJ, Sekiguchi JM, Rathbun GA, Swat W, Wang J, Bronson RT, Malynn BA, Bryans M, Zhu C, Chaudhuri J, Davidson L, Ferrini R, Stamato T, Orkin SH, Greenberg ME, Alt FW. A critical role for DNA end-joining proteins in both lymphogenesis and neurogenesis. Cell 1998b;95:891–902. [PubMed: 9875844]

Goodarzi AA, Yu Y, Riballo E, Douglas P, Walker SA, Ye R, Harer C, Marchetti C, Morrice N, Jeggo PA, Lees-Miller SP. DNA-PK autophosphorylation facilitates Artemis endonuclease activity. EMBO J 2006;25:3880–3889. [PubMed: 16874298]

Gu J, Lu H, Tsai AG, Schwarz K, Lieber MR. Single-stranded DNA ligation and XLF-stimulated incompatible DNA end ligation by the XRCC4-DNA ligase IV complex: influence of terminal DNA sequence. Nucleic Acids Res 2007;35:5755–5762. [PubMed: 17717001]

Hentges P, Ahnesorg P, Pitcher RS, Bruce CK, Kysela B, Green AJ, Bianchi J, Wilson TE, Jackson SP, Doherty AJ. Evolutionary and Functional Conservation of the DNA Non-homologous End-joining Protein, XLF/Cernunnos. J. Biol. Chem 2006;281:37517–37526. [PubMed: 17038309]

Lee Y, McKinnon PJ. Responding to DNA double strand breaks in the nervous system. Neuroscience. 2006

Lee Y, McKinnon PJ. DNA ligase IV suppresses medulloblastoma formation. Cancer Res 2002;62:6395–6399. [PubMed: 12438222]

Li Y, Chirgadze DY, Bolanos-Garcia VM, Sibanda BL, Davies OR, Ahnesorg P, Jackson SP, Blundell TL. Crystal structure of human XLF/Cernunnos reveals unexpected differences from XRCC4 with implications for NHEJ. EMBO J. 2007

Lu H, Pannicke U, Schwarz K, Lieber MR. Length-dependent binding of human XLF to DNA and stimulation of XRCC4.DNA ligase IV activity. J. Biol. Chem 2007;282:11155–11162. [PubMed: 17317666]

Ma Y, Pannicke U, Schwarz K, Lieber MR. Hairpin opening and overhang processing by an Artemis/DNA-dependent protein kinase complex in nonhomologous end joining and V(D)J recombination. Cell 2002;108:781–794. [PubMed: 11955432]

Mills KD, Ferguson DO, Essers J, Eckersdorff M, Kanaar R, Alt FW. Rad54 and DNA Ligase IV cooperate to maintain mammalian chromatid stability. Genes Dev 2004;18:1283–1292. [PubMed: 15175260]

Moshous D, Callebaut I, de Chasseval R, Corneo B, Cavazzana-Calvo M, le Deist F, Tezcan I, Sanal O, Bertrand Y, Philippe N, Fischer A, de Villartay JP. Artemis, a novel DNA double-strand break repair/V(D)J recombination protein, is mutated in human severe combined immune deficiency. Cell 2001;105:177–186. [PubMed: 11336668]

Mostoslavsky R, Chua KF, Lombard DB, Pang WW, Fischer MR, Gellon L, Liu P, Mostoslavsky G, Franco S, Murphy MM, Mills KD, Patel P, Hsu JT, Hong AL, Ford E, Cheng HL, Kennedy C, Nunez N, Bronson R, Frendewey D, Auerbach W, Valenzuela D, Karow M, Hottiger MO, Hursting S, Barrett JC, Guarente L, Mulligan R, Demple B, Yancopoulos GD, Alt FW. Genomic instability and aging-like phenotype in the absence of mammalian SIRT6. Cell 2006;124:315–329. [PubMed: 16439206]

Nussenzweig A, Chen C, da CS, V Sanchez M, Sokol K, Nussenzweig MC, Li GC. Requirement for Ku80 in growth and immunoglobulin V(D)J recombination. Nature 1996;382:551–555. [PubMed: 8700231]

Rooney S, Sekiguchi J, Zhu C, Cheng HL, Manis J, Whitlow S, DeVido J, Foy D, Chaudhuri J, Lombard D, Alt FW. Leaky Scid phenotype associated with defective V(D)J coding end processing in Artemis-deficient mice. Mol. Cell 2002;10:1379–1390. [PubMed: 12504013]

Rossi DJ, Bryder D, Seita J, Nussenzweig A, Hoeijmakers J, Weissman IL. Deficiencies in DNA damage repair limit the function of haematopoietic stem cells with age. Nature 2007;447:725–729. [PubMed: 17554309]

Shinkai Y, Rathbun G, Lam KP, Oltz EM, Stewart V, Mendelsohn M, Charron J, Datta M, Young F, Stall AM. RAG-2-deficient mice lack mature lymphocytes owing to inability to initiate V(D)J rearrangement. Cell 1992;68:855–867. [PubMed: 1547487]

Stavnezer J, Guikema JE, Schrader CE. Mechanism and Regulation of Class Switch Recombination. Annu. Rev. Immunol 2008;26:261–292. [PubMed: 18370922]261–292

Teo SH, Jackson SP. Lif1p targets the DNA ligase Lig4p to sites of DNA double-strand breaks. Curr. Biol 2000;10:165–168. [PubMed: 10679327]

Tsai CJ, Kim SA, Chu G. Cernunnos/XLF promotes the ligation of mismatched and noncohesive DNA ends. Proc. Natl. Acad. Sci. U. S. A 2007;104:7851–7856. [PubMed: 17470781]

Wang Q, Gao F, May WS, Zhang Y, Flagg T, Deng X. Bcl2 negatively regulates DNA double-strand-break repair through a nonhomologous end-joining pathway. Mol. Cell 2008;29:488–498. [PubMed: 18313386]

Weill JC, Reynaud CA. DNA polymerases in adaptive immunity. Nat. Rev. Immunol 2008;8:302–312. [PubMed: 18340343]

Yan C, Souza EK, Franco S, Hickernell T, Boboila C, Gumaste S, Geyer M, Alimzhanov M, Manis J, Rajewsky K, Alt FW. IgH Class Switching and Chromosomal Translocations Employ a Robust Non-classical End-joining Pathway. 2007Submitted

Yan CT, Kaushal D, Murphy M, Zhang Y, Datta A, Chen C, Monroe B, Mostoslavsky G, Coakley K, Gao Y, Mills KD, Fazeli AP, Tepsuporn S, Hall G, Mulligan R, Fox E, Bronson R, De Girolami U, Lee C, Alt FW. XRCC4 suppresses medulloblastomas with recurrent translocations in p53-deficient mice. Proc. Natl. Acad. Sci. U. S. A 2006;103:7378–7383. [PubMed: 16670198]

Young F, Mizoguchi E, Bhan AK, Alt FW. Constitutive Bcl-2 expression during immunoglobulin heavy chain-promoted B cell differentiation expands novel precursor B cells. Immunity 1997;6:23–33. [PubMed: 9052834]

Zha S, Alt FW, Cheng HL, Brush JW, Li G. Defective DNA repair and Increased Genomic Instability in Cernunnos-XLF-deficient Murine Embryonic Stem Cells. Proc Natl Acad Sci U S A. 2007

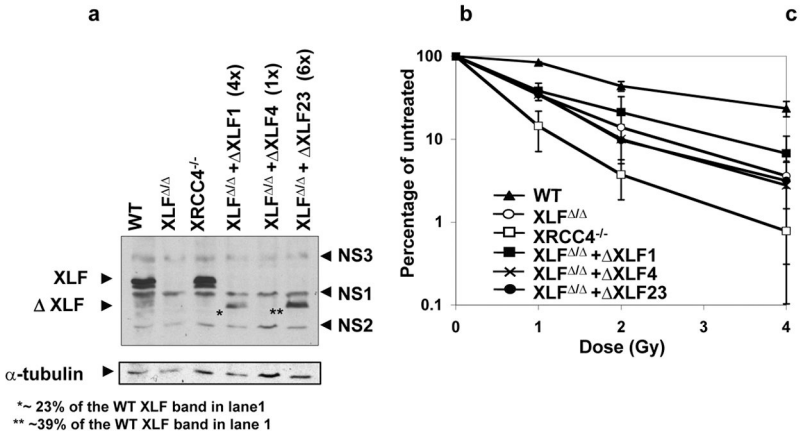

c

Cell line	Relative level	Fidelity
Signal join		
WT	100%	100%
XLF$^{\Delta/\Delta}$	4.1-9.8%	75%
XLF$^{\Delta/\Delta}$ +ΔXLF	1.2-5.2%	N.D.
XRCC4^{-}	<1.8%	N.D.
No Rag	<0.6%	N.D.
Coding join		
WT	100%	
XLF$^{\Delta/\Delta}$	4.7-9.5%	
XLF$^{\Delta/\Delta}$ +ΔXLF	4.7-8.0%	
XRCC4^{-}	<3.9%	
No Rag	<0.4%	

Figure 1. Characterization of XLF$^{\Delta/\Delta}$ ES cells

(A) Western blotting assay for XLF in WT, XLF$^{\Delta/\Delta}$ and XLF$^{\Delta/\Delta}$ ES cells that over-express truncated XLF. The number in the brackets indicates the cDNA construct copy number in each line. "XLF" denotes the mobility of authentic XLF while "ΔXLF" denotes the mobility of XLF$^{\Delta\alpha4/5}$. NS1, 2 and 3 indicate mobility of commonly observed non-specific bands observed in WT and XLF$^{\Delta/\Delta}$ extracts. The * and ** symbols denote XLF$^{\Delta\alpha4/5}$ bands from 4 and 6 copy transfectants, respectively (B) IR sensitivity of WT, XLF$^{\Delta/\Delta}$ ES cells and XLF$^{\Delta/\Delta}$ ES over-expressing XLF$^{\Delta\alpha4/5}$ from a pGK-promoter based expression vector. (C) Summary of transient V(D)J recombination results on WT, XLF$^{\Delta/\Delta}$ and XLF$^{\Delta/\Delta}$ ES cells that over-expressed XLF$^{\Delta\alpha4/5}$ Values reflect two independent experiments from two independent XLF$^{\Delta\alpha4/5}$ over-expressing ES lines (6 and 4 copies; see Table S1 for details).

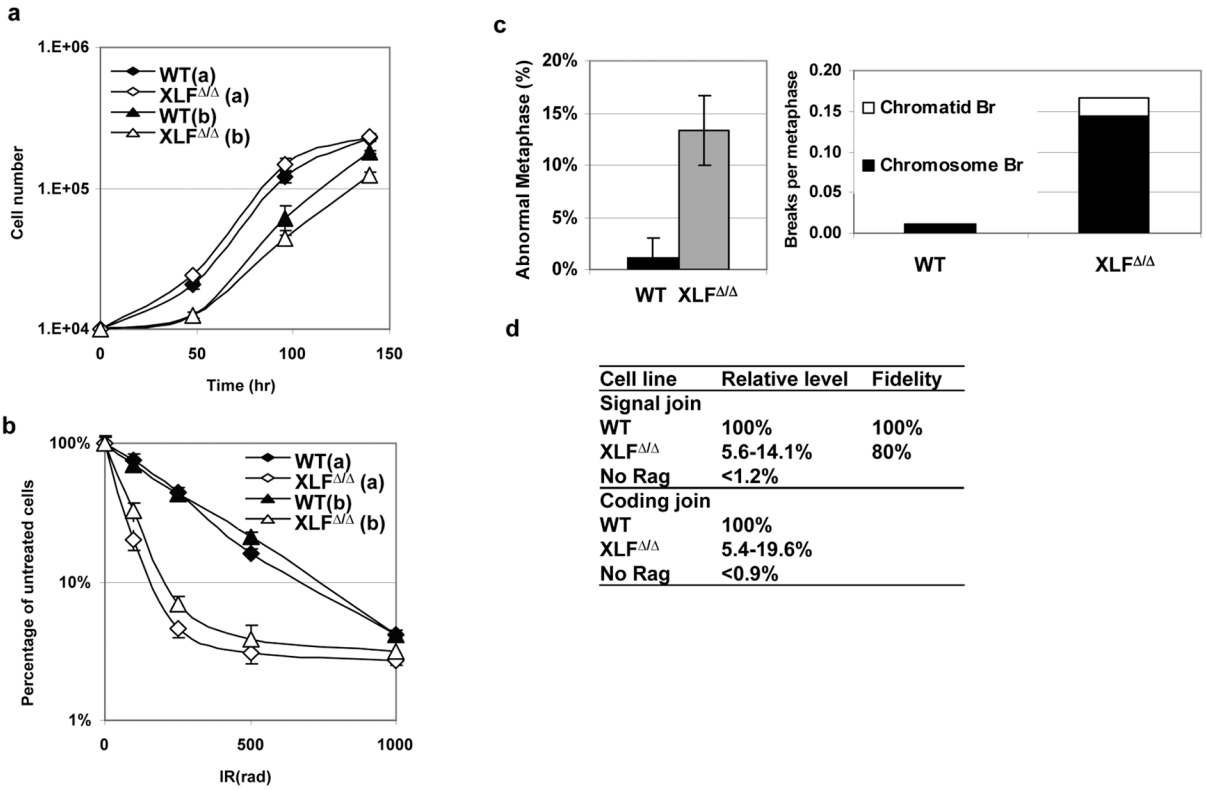

Cell line	Relative level	Fidelity
Signal join		
WT	100%	100%
XLF$^{\Delta/\Delta}$	5.6-14.1%	80%
No Rag	<1.2%	
Coding join		
WT	100%	
XLF$^{\Delta/\Delta}$	5.4-19.6%	
No Rag	<0.9%	

Figure 2. Characterization of XLF$^{\Delta/\Delta}$ MEFs

(A) Proliferation of two independent sets (set a from 129/Sv background and set b from 129/BL6 mixed background) of primary WT and XLF$^{\Delta/\Delta}$ MEFs. (B) IR sensitivity of the two independent sets of WT and XLF$^{\Delta/\Delta}$ MEFs. (C) T- FISH analyses of spontaneous cytogenetic abnormalities in passage one WT and XLF$^{\Delta/\Delta}$ MEF lines (n=3 for each genotype). Chromosome and chromatid breaks were scored as descried (Franco et al., 2008). (D) Transient V(D)J recombination results from immortalized WT and XLF$^{\Delta/\Delta}$ MEFs. Values were obtained from multiple independent experiments from two independent XLF$^{\Delta/\Delta}$ MEF lines (see Sup. Fig. 3 and Table S2 for details).

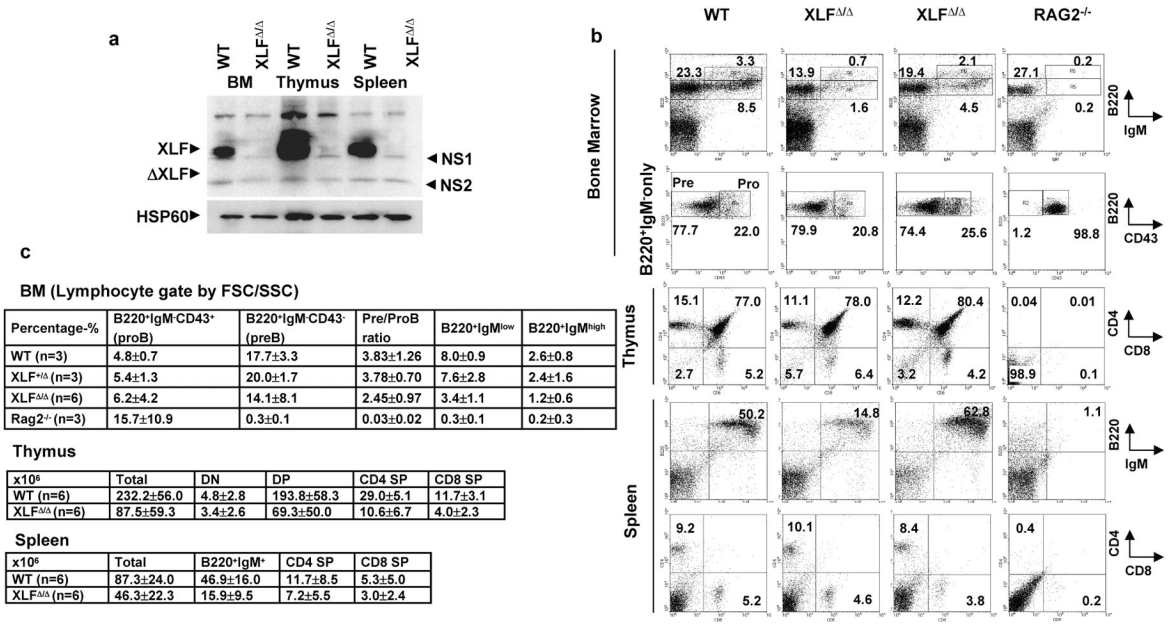

c

BM (Lymphocyte gate by FSC/SSC)

Percentage-%	B220+IgM-CD43+ (proB)	B220+IgM-CD43- (preB)	Pre/ProB ratio	B220+IgMlow	B220+IgMhigh
WT (n=3)	4.8±0.7	17.7±3.3	3.83±1.26	8.0±0.9	2.6±0.8
XLF+/Δ (n=3)	5.4±1.3	20.0±1.7	3.78±0.70	7.6±2.8	2.4±1.6
XLFΔ/Δ (n=6)	6.2±4.2	14.1±8.1	2.45±0.97	3.4±1.1	1.2±0.6
Rag2-/- (n=3)	15.7±10.9	0.3±0.1	0.03±0.02	0.3±0.1	0.2±0.3

Thymus

x10⁶	Total	DN	DP	CD4 SP	CD8 SP
WT (n=6)	232.2±56.0	4.8±2.8	193.8±58.3	29.0±5.1	11.7±3.1
XLFΔ/Δ (n=6)	87.5±59.3	3.4±2.6	69.3±50.0	10.6±6.7	4.0±2.3

Spleen

x10⁶	Total	B220+IgM+	CD4 SP	CD8 SP
WT (n=6)	87.3±24.0	46.9±16.0	11.7±8.5	5.3±5.0
XLFΔ/Δ (n=6)	46.3±22.3	15.9±9.5	7.2±5.5	3.0±2.4

Figure 3. Lymphocyte Development in XLF$^{\Delta/\Delta}$ Mice

(A) Western blotting analysis of XLF cross-reactive protein expression in extracts from indicated lymphoid organs of littermate-matched WT and XLF$^{\Delta/\Delta}$ mice (see Sup. Fig. 1 for more examples). Symbols are as described in Fig. 1 legend. (B) Representative FACS analyses of lymphocyte development in four week old WT, XLF$^{\Delta/\Delta}$ and RAG2$^{-/-}$ mice. (C) Percentage and number of developing and mature lymphocytes in bone marrow, thymus and spleen from WT and XLF$^{\Delta/\Delta}$ mice. Cell numbers in different fractions indicated in panel C were calculated by determining total cell numbers in each organ and then determining the percentage in each fraction (indicated by boxes on FACS plots in panel B).

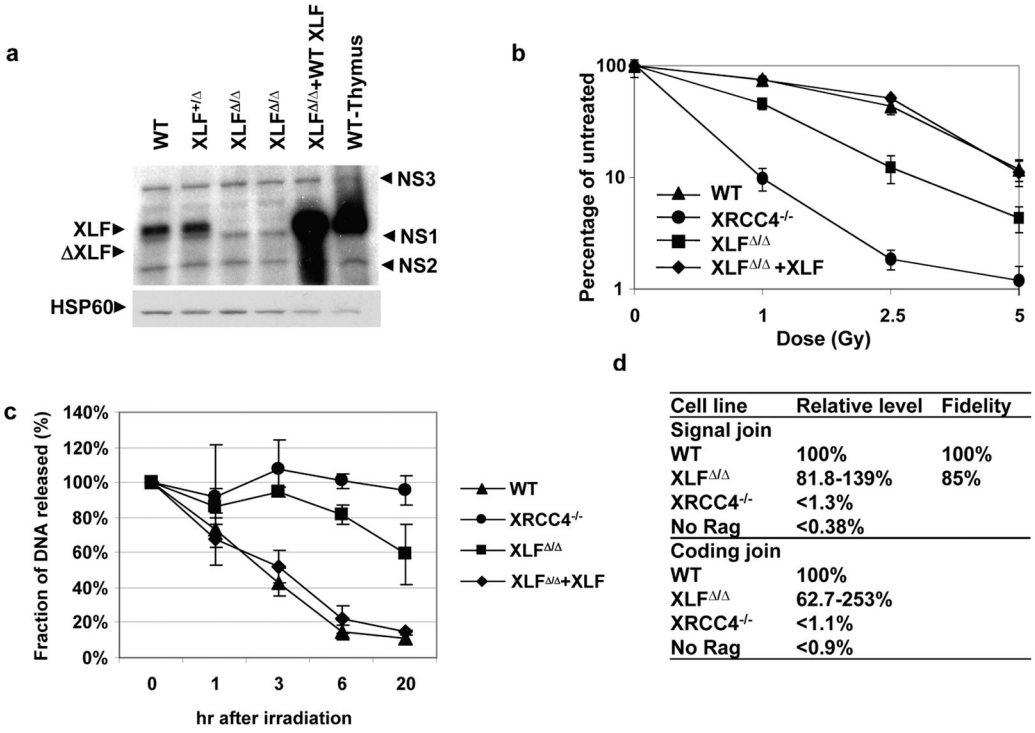

Cell line	Relative level	Fidelity
Signal join		
WT	100%	100%
XLF$^{\Delta/\Delta}$	81.8-139%	85%
XRCC4$^{-/-}$	<1.3%	
No Rag	<0.38%	
Coding join		
WT	100%	
XLF$^{\Delta/\Delta}$	62.7-253%	
XRCC4$^{-/-}$	<1.1%	
No Rag	<0.9%	

Figure 4. Characterization of XLF$^{\Delta/\Delta}$ A-MuLV Transformed Pro-B cells

(A) Western blotting for XLF expression in WT and XLF$^{\Delta/\Delta}$ A-MuLV transformed pro-B cells and XLF$^{\Delta/\Delta}$ A-MuLV transformant that over-expresses WT XLF from an integrated SV40-promoter based vector containing a puromycin resistant gene (denoted as XLF$^{\Delta/\Delta}$ +XLF). See Sup. Figure 1 for more examples. (B) IR sensitivity of WT, XLF$^{\Delta/\Delta}$ and XLF$^{\Delta/\Delta}$ +XLF A-MuLV transformed pro-B cells. (C) Repair of IR induced DNA DSBs by WT, XLF$^{\Delta/\Delta}$ and XLF$^{\Delta/\Delta}$ +XLF A-MuLV transformed pro-B cells. The average and standard deviation of three experiments are plotted. (D) Summary of the transient V(D)J recombination assays on WT, XLF$^{\Delta/\Delta}$ and XLF$^{\Delta/\Delta}$ +XLF A-MuLV transformed pro-B cells (see Sup. Fig. 7 and Table S3 for details).

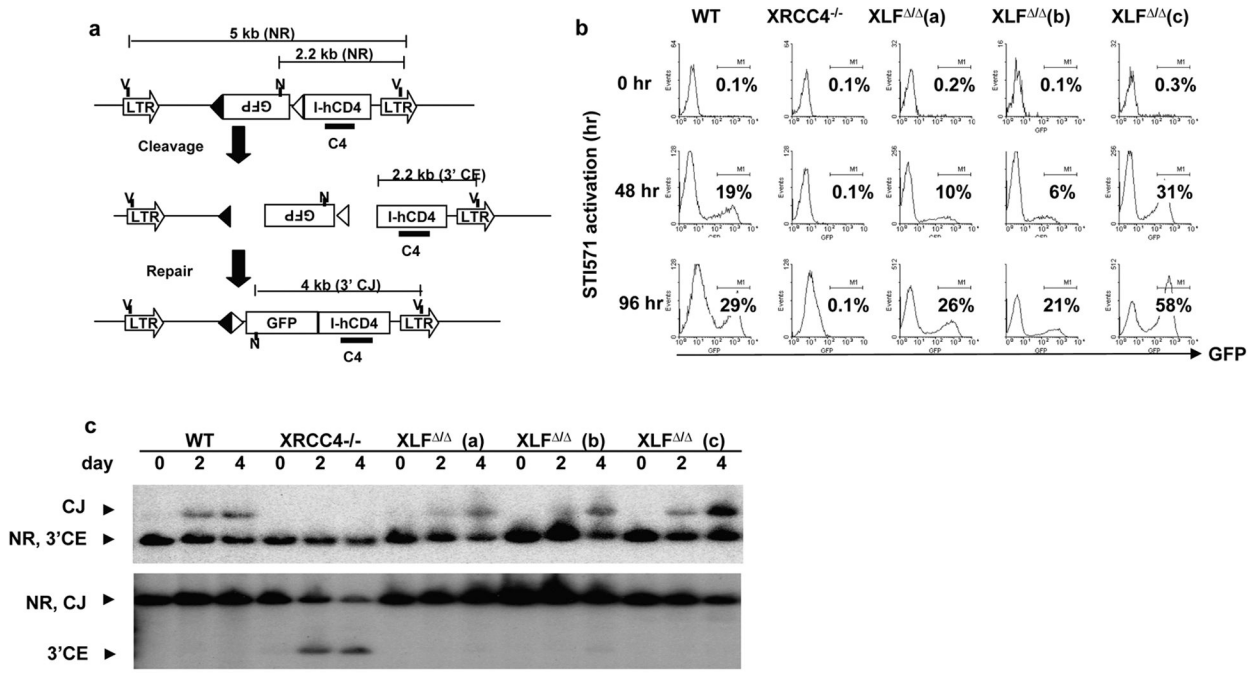

Figure 5. Chromosomal V(D)J Recombination in WT and XLF$^{\Delta/\Delta}$ A-MuLV Transformants

(A) The pMX-INV V(D)J recombination substrate (adapted from Bredemeyer et al., 2006). The pMX-INV vector has a single pair of recombination RSs that flank an inverted green fluorescent protein (GFP) cassette. Normal V(D)J recombination allows for GFP expression. Also shown is a schematic representation of non-rearranged (NR), cleavage intermediates (CE and SE) and joining products (CJ and SJ) of pMX-INV. The long terminal repeats (LTR), packaging sequence, GFP cDNA, IRES-hCD4 cDNA (I-hCD4), 5' 12-recombination signal (12-RS) and 3' 23-RS (filled and open triangles, respectively), EcoRV (V) site, NcoI (N) site, and C4 probe are indicated. (B) Clones of WT, XRCC4$^{-/-}$ and three independent XLF$^{\Delta/\Delta}$ (a, b, and c) pro-B cell lines were treated with STI571 for 0, 48 and 96 hours and rearrangement was assayed for GFP expression. (C) Southern blot analyses of the rearrangement status of an inversional V(D)J recombination substrate (on right). For the upper gel, DNA was digested with EcoRV and NcoI and probed with the indicated C4 probe. The NR (non-rearranged) and 3'CE are both 2.2kb and the rearranged product is 4kb. For the lower gel, DNA was digested with EcoRV and probed with the same C4 probe. The NR and CJ are 5 kb bands and the 3'CE is a 2.2 kb band.

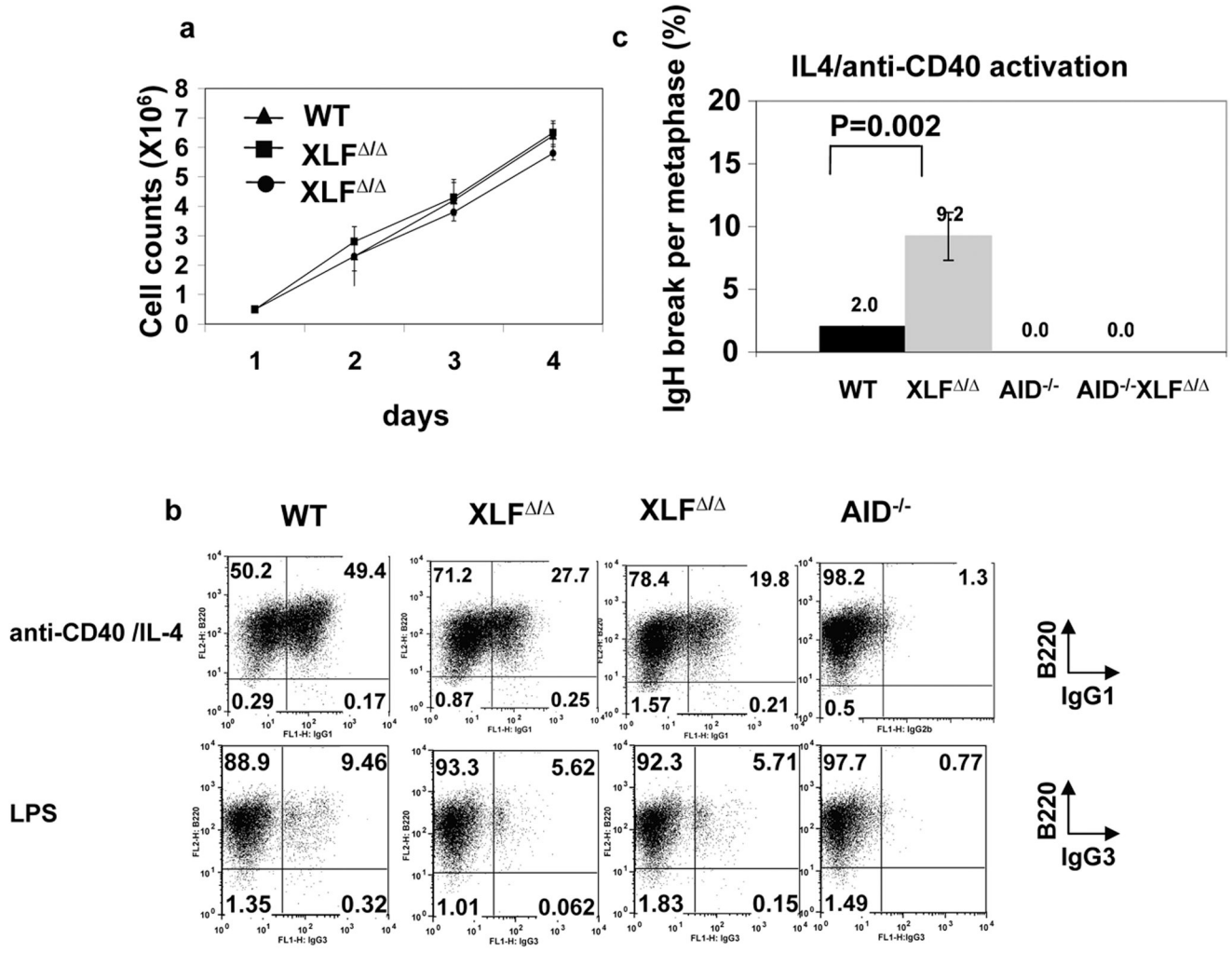

Figure 6. Class Switch Recombination in XLF$^{\Delta/\Delta}$ Mice

(A) Proliferation of purified splenic B cells from WT and XLF$^{\Delta/\Delta}$ mice following αCD40/IL-4 stimulation. (B) Representative FACS analysis of CD43^{-} splenocytes from WT, AID$^{-/-}$ and XLF$^{\Delta/\Delta}$ mice after a four-days of indicated stimulations. (C) Percentage of IgH locus breaks measured by IgH locus-specific FISH in WT, XLF$^{\Delta/\Delta}$ AID$^{-/-}$ and XLF$^{\Delta/\Delta}$ AID$^{-/-}$ B metaphases after cells were stimulated for 4 days with αCD40/IL-4. Data represent the average and standard deviation from multiple experiments.